2

INSTITUTE FOR FUSION STUDIES

DOE/ET-53088-576 IFSR #576

Magnetic Reconnection at Stressed X-Type Neutral Points

L. OFMAN, P.J. MORRISON, and R.S. STEINOLFSON

Institute for Fusion Studies
The University of Texas at Austin
Austin, Texas 78712

October 1992

THE UNIVERSITY OF TEXAS

AUSTIN

DISCLAIMER

Magnetic Reconnection at Stressed X-Type Neutral Points

DOE/ET/53088--576

DE93 002167

L. Ofman,[a] P.J. Morrison
Department of Physics and
Institute for Fusion Studies
The University of Texas at Austin
Austin, Texas 78712
and
R.S. Steinolfson
Department of Space Sciences
Southwest Research Institute
San Antonio, Texas 78228

Abstract

The reconnection and relaxation of two-dimensional stressed (non-potential) x-type neutral point magnetic fields are studied via solution of the nonlinear resistive 2-D MHD equations and by analytical solution of the linear eigenvalue problem. Previous linear studies [I. Craig and A. McClymont, Ap. J. **371**, L41 (1991); A. Hassam, Preprint UMLPR 92-046, Univ. of Maryland (1991); Craig and Watson, Ap. J. **393**, 385 (1992)] have shown that such stressed fields may relax on a time substantially shorter (i.e. $\sim |\log \eta|$, where η is the resistivity) than the usual time scale for linear reconnection (i.e. $\eta^{3/5}$). We have generalized the linear dispersion relation for azimuthally non-symmetric perturbations, and have found that for modes with azimuthal mode numbers $m > 0$, the relaxation can occur at a rate faster than that for $n = m = 0$, where n is the

[a]Present address: NASA Goddard Space Flight Center, Code 682.1, Greenbelt, MD 20771

radial "quantum" number. We find that for nearly azimuthally symmetric magnetic perturbations that are zero at the boundary; i.e. the "frozen-in" (sometimes called "line-tied") boundary conditions, the fields relax incompressibly and nonlinearly to the unstressed x-type neutral point at a rate close to that predicted by linear theory. Also, fully compressible nonlinear MHD simulations have been performed, which show that the interaction between the plasma flow velocity and the magnetic field is the important physical effect, while the inclusion of thermodynamics does not affect the evolution considerably. A Lyapunov functional for the nonlinear incompressible 2-D resistive MHD equations is derived to show that the current-free x-point configuration is a global equilibrium to which general initial conditions relax.

I. Introduction

Magnetic reconnection is believed to occur in solar coronal loops, the magnetopause boundary, the solar wind, extragalactic jets and fusion experiments. Giovanelli (1947) was the first to observe that solar flares frequently occur near magnetic neutral points. Based on these observations Dungey (1953, 1958) proposed an x-type neutral point mechanism for particle acceleration, the onset of sheet currents, and the energy release in solar flares, provided that the magnetic field sources are free to move. Chapman and Kendall (1962) solved the nonlinear ideal MHD equations for the x-type neutral point and found growth on an Alfvén time scale, while Syrovatsky (1966) included the mechanism in a solar flare model. Sweet (1958) and Parker (1963) used dimensional arguments for a model involving merging of antiparallel magnetic fields, and concluded that the reconnection rate scales as $\eta^{1/2}$, while Petschek (1964) predicted an Alfvénic reconnection rate based on semi-quantitative Alfvén shock wave solutions. Furth, Killeen and Rosenbluth (1963) developed an analytic boundary layer theory, and derived the $\eta^{3/5}$ linear tearing growth rate scaling, while Rutherford (1973) considered the nonlinear stage and found that the reconnected flux $\Phi \sim \eta t$ and the reconnection rate diminishes from an exponential to an algebraic rate. Recently, Hassam (1991) has considered an x-point magnetic field configuration with the frozen-in boundary conditions and has analytically solved the linearized compressible low-beta MHD equations, for azimuthally symmetric $m = 0$ modes. Craig and McClymont (1991), and Craig and Watson (1992) numerically solved the linearized low-beta MHD equations for this problem. They found that the perturbed x-point magnetic configuration relaxes to the potential (current-free) x-point with an intermediate decay rate that is slower than the Alfvén rate, but faster than the resistive diffusion rate. Experimental studies by Bratenahl and Yeates (1970), Baum and Bratenahl (1974a,b), Baum *et al.* (1973a,b) found that the initially perturbed x-type

magnetic field configuration rapidly relaxes to the potential state. For a detailed review see for example Priest (1981), Syrovatsky (1981) and reference therein.

Here we solve the 2-D nonlinear resistive MHD equations for both fully compressible (without restrictions on the value of the pressure) and incompressible plasma with the frozen-in boundary condition. Both the linear and nonlinear relaxation rates of the stressed (perturbed) x-point back to the potential x-point configuration are obtained. In addition we have obtained a general dispersion relation that includes the azimuthally non-symmetric $m > 0$ modes, as well as the $m = 0$ mode, and have compared the results of the linear dispersion relation with the nonlinear simulations. By considering both compressible and incompressible dynamics we show that the physics is dominated by the coupling of the magnetic field to the inertial terms, and that thermodynamics plays a minimal role. Finally, we obtain a Lyapunov functional for the nonlinear incompressible 2-D resistive MHD equations, which shows that the potential x-point with the frozen-in boundary conditions is an equilibrium state to which all initial conditions relax.

The effect of free boundary conditions; i.e. where the plasma is allowed to flow through the boundary and where the magnetic field at the boundary is free to adjust, was considered in a separate study (Ofman, 1992; Steinolfson *et al.*, 1992.) There it was found for the free boundary conditions that the x-point evolves into a current sheet and the perturbation grows (rather than relaxes) on an Alfvén time scale.

This paper is organized as follows: In § 2 the basic MHD equations for our model, and the initial magnetic field configuration are presented. In § 3 we derive the linear dispersion relation. The numerical results of the nonlinear MHD simulations are presented in § 4, and the Lyapunov relaxation arguments are given in §-5. The summary and discussion are in § 6.

II. Incompressible 2-D MHD Equations

We assume that collisional MHD theory (Drake and Lee, 1977) is applicable, that the plasma resistivity η is constant and isotropic, and that gravitational and viscous effects are negligible. With these assumptions the basic equations in cgs units are:

$$\rho\left[\frac{\partial \mathbf{v}}{\partial t} + (\mathbf{v}\cdot\nabla)\mathbf{v}\right] = -\nabla P + \frac{1}{4\pi}(\nabla\times\mathbf{B})\times\mathbf{B} \tag{1}$$

$$\frac{\partial \mathbf{B}}{\partial t} = \nabla\times(\mathbf{v}\times\mathbf{B}) - \frac{c^2\eta}{4\pi}\nabla\times(\nabla\times\mathbf{B}) \tag{2}$$

$$\frac{\partial \rho}{\partial t} + \nabla\cdot(\rho\mathbf{v}) = 0 \tag{3}$$

$$\nabla\cdot\mathbf{B} = 0 \tag{4}$$

$$\frac{d}{dt}\left(\frac{p}{\rho^{\gamma_p}}\right) = 0\ , \tag{5}$$

where c is the speed of light, ρ is the plasma density, $\mathbf{B}$ is the magnetic field, $\mathbf{v}$ is the velocity field, P is the pressure, and γ_p is the polytropic index. We use Eqs. (1)-(5) with the equilibrium of Eq. (8) below. Assuming that the evolution is two-dimensional ($\frac{\partial}{\partial z} = 0$), the above set of equations is solved using three separate approaches:

1. Solution of the dispersion relation arising from the linearized Eqs. (1)-(4) with the assumption $\nabla P = 0$ in Eq. (1).

2. Numerical solution of the 2-D MHD equations in slab geometry given below-in Eqs. (9) and (10), which are obtained from Eqs. (1)-(4) with the assumption of incompressibility ($\nabla\cdot\mathbf{v} = 0$).

3. Numerical solution of the compressible MHD Equations (1)-(3) and Eq. (5) in the (r,θ) plane without any further approximations [Eq. (4) is not solved explicitly].

The linearized equations resulting from the first approach and their solution will be presented in § III. In the remainder of this section we present the equations needed for the second approach.

In two dimensions the magnetic and velocity fields can be written as

$$\mathbf{B} = \nabla\Psi \times \mathbf{e}_z \tag{6}$$

$$\mathbf{V} = \nabla\phi \times \mathbf{e}_z \tag{7}$$

where Ψ and ϕ are the flux and stream functions, respectively, and $\Psi = \psi_E + \psi$ with the equilibrium stream function ψ_E given by

$$\psi_E = B_0(x^2 - y^2)/2a \ . \tag{8}$$

The contour lines of ψ_E (which are parallel to the magnetic field lines) are shown in Fig. 1. Next, substituting Eqs. (6)-(8) into Eqs. (1) and (2) with $\rho = \rho_0 = \text{const.}$, and taking the curl of Eq. (1) to eliminated the pressure P, yields the following set of equations, which we write in dimensionless form:

$$\frac{\partial\psi}{\partial t} = -\frac{\partial\phi}{\partial y}\left(\frac{\partial\psi}{\partial x} + x\right) + \left(\frac{\partial\psi}{\partial y} - y\right)\frac{\partial\phi}{\partial x} - \frac{1}{S}J \tag{9}$$

$$\frac{\partial\omega}{\partial t} = -\frac{\partial\phi}{\partial y}\frac{\partial\omega}{\partial x} + \frac{\partial\phi}{\partial x}\frac{\partial\omega}{\partial y} + \left(\frac{\partial\psi}{\partial y} - y\right)\frac{\partial J}{\partial x} - \left(\frac{\partial\psi}{\partial x} + x\right)\frac{\partial J}{\partial y} \ , \tag{10}$$

where $J = -\nabla_\perp^2\psi$ is the z-component of the current, $\omega = -\nabla_\perp^2\phi$ is the z-component of the vorticity, and $\nabla_\perp^2 \equiv \frac{\partial^2}{\partial x^2} + \frac{\partial^2}{\partial y^2}$ with $\frac{\partial}{\partial z} = 0$. The time is normalized to the Alfvén time $\tau_h = a_b(4\pi\rho_0)^{1/2}/B_0$, the coordinates are scaled by the characteristic magnetic field length a_b, and B_0 is the average magnitude of the magnetic field at the boundary. The dimensionless parameter in these equations is the magnetic Reynolds number $S = \tau_r/\tau_h$, where $\tau_r = 4\pi a_b^2/c^2\eta$ is the resistive diffusion time. We have also assumed that the equilibrium magnetic field is maintained by an external electric field (i.e., the equilibrium magnetic field is not

dissipated resistively). In § IV we present the numerical results obtained with Eqs. (9) and (10).

III. Linear Dispersion Relation

Neglecting the pressure gradient and linearizing the MHD equations around the equilibrium quantities ψ_E, $\rho_0 = 1$, and $\mathbf{v}_0 = 0$, yields with Eqs. (1)-(3)

$$\frac{\partial \rho}{\partial t} + \nabla \cdot \mathbf{v} = 0 \tag{11}$$

$$\frac{\partial \mathbf{v}}{\partial t} = -\nabla \psi_E \nabla^2 \psi \tag{12}$$

$$\frac{\partial \psi}{\partial t} + \mathbf{v} \cdot \nabla \psi_E = S^{-1} \nabla^2 \psi \ , \tag{13}$$

where ψ, ρ, and $\mathbf{v}$ denote perturbations of the equilibrium quantities.

Next, upon multiplying Eq. (12) by $\nabla \psi_E$, Eqs. (11)-(13) can be combined into a single equation for ψ,

$$\frac{\partial^2 \psi}{\partial t^2} - S^{-1} \frac{\partial}{\partial t} \nabla^2 \psi = |\nabla \psi_E|^2 \nabla^2 \psi \ , \tag{14}$$

where $|\nabla \psi_E|^2 = r^2 = x^2 + y^2$. The diffusion term in Eq. (14) is dominant when $r \ll r_c$, where $r_c = \eta^{1/2}$ is the skin depth. Assuming the following separation of variables in cylindrical geometry $\psi(r, \theta, t) = e^{-\gamma t} f(r) e^{im\theta}$, the eigenvalue equation for $f(r)$ becomes

$$r \frac{d}{dr} \left(r \frac{df}{dr} \right) = \left(\frac{\gamma^2}{1 - \gamma / S r^2} + m^2 \right) f \ , \tag{15}$$

and the radial part of the current $\mathbf{j} = -\nabla^2 \psi \, \mathbf{e}_z$ is given by

$$j(r) = \frac{\gamma^2}{\gamma / S - r^2} f(r) \ . \tag{16}$$

The frozen-in boundary condition is given by

$$f(r = 1) = \psi(r = 1, \theta) = 0 \ . \tag{17}$$

Equation (15) is mapped into the hypergeometric equation by the transformations $z = r^2 S/\gamma$, and $f = z^\alpha \xi$:

$$z(z-1)\xi'' + (m+1)(z-1)\xi' - \gamma^2/4\xi = 0 \ , \tag{18}$$

where we have set $\alpha = m/2$. The solution of Eq. (18) that is regular at $r = 0$ is the hypergeometric function $F(a, b, c, z)$ with $a = m/2 + \Delta/2$, $b = m/2 - \Delta/2$, $c = m + 1$, and $\Delta = \sqrt{m^2 + \gamma^2}$. From the boundary condition (17) we obtain the dispersion relation,

$$F(m/2 + \Delta/2, m/2 - \Delta/2, m + 1, S/\gamma) = 0 \ . \tag{19}$$

For the cases of interest, $|z| = |S/\gamma| > 1$; hence, the transformation formula (Oberhettinger, 1972),

$$F(a,b,c,z) = \frac{\Gamma(c)\Gamma(b-a)}{\Gamma(b)\Gamma(c-a)}(-z)^{-a}F(a, 1-c+a, 1-b+a, 1/z) +$$

$$+\frac{\Gamma(c)\Gamma(a-b)}{\Gamma(a)\Gamma(c-b)}(-z)^{-b}F(b, 1-c+b, 1-a+b, 1/z), \ |\arg(-z)| < \pi \tag{20}$$

is needed to obtain the dispersion relation. Substituting the values of a, b, and c, using the properties of the Gamma function, and using Eq. (19) yields the following linear dispersion relation for the reconnecting x-point:

$$\frac{(m+\Delta)\Gamma(-\Delta)\Gamma^2(m/2+\Delta/2)}{(m-\Delta)\Gamma(\Delta)\Gamma^2(m/2-\Delta/2)} =$$

$$= -\left(-\frac{S}{\gamma}\right)^{\Delta} \frac{F(m/2-\Delta/2, -m/2-\Delta/2, 1-\Delta, \gamma/S)}{F(m/2+\Delta/2, -m/2+\Delta/2, 1+\Delta, \gamma/S)} \tag{21}$$

Equation (21) can be further simplified with the assumption $\gamma/S \ll 1$, which results in the following, upon asymptotically expanding the right-hand side of (21)

$$\frac{(m+\Delta)\Gamma(-\Delta)\Gamma^2(m/2+\Delta/2)}{(m-\Delta)\Gamma(\Delta)\Gamma^2(m/2-\Delta/2)} \approx -\left(-\frac{S}{\gamma}\right)^{\Delta} \frac{1 + \frac{\gamma^3}{4S(1-\Delta)}}{1 + \frac{\gamma^3}{4S(1+\Delta)}} \ . \tag{22}$$

A special case of this dispersion relation, that for $n = m = 0$ was derived by Hassam (1991). When $m = n = 0$ and in the limit $|\gamma| \ll 1$, the dispersion relation (21) can be

approximated by the following asymptotic expressions:

$$\mathrm{Im}\ \gamma \sim \frac{\pi}{\log S}\left[1 - \frac{\log(\log S))}{\log S}\right] \tag{23}$$

$$\mathrm{Re}\ \gamma \sim \frac{\psi/2}{\log S}\,\mathrm{Im}\ \gamma \sim \frac{\pi^2}{2(\log S)^2}\ . \tag{24}$$

We have solved the dispersion relation (21) numerically for both $m = 0$, and $m \neq 0$, with S varying over several orders of magnitude. Values of γ from Eqs. (23) and (24) were used as initial guesses in our numerical solution of the exact dispersion relation. The resulting decay rates and their dependence on S, with $m = n = 0$ and $n = 1,\ m = 2, 4$ are shown in Fig. 2. The near linear dependence for the various modes agrees with the $\log S$ scaling of Eqs. (23) and (24).

The real and imaginary parts of the eigenfunction $f(r)$, and the radial part of the current $j(r)$ with $m = 0$, $n = 1$, $S = 10^3$ and $m = 1$, $n = 3$, $S = 10^5$ are presented in Fig. 3. The "quantum" number n determines the number of radial nodes of $f(r)$ in the interval $r \in (0, 1)$. When $m = 0$, $\mathrm{Re}\{f(r)\}$ approaches a constant as $r \to 0$ and when $m = 1$, $f(r \to 0) \to 0$. It is evident from Eq. (16) that the current j becomes proportional to $f(r)$ as r approaches zero, therefore for the $m = 0$ mode $j(r \to 0) \to$ const., and for the $m = 1$ mode $j(r \to 0) \to 0$. The $m > 0$ modes are not associated with reconnection at the x-point in agreement with previous studies (Hassam, 1991; Craig and McClymont, 1991; Craig and Watson, 1992); however, these modes decouple the fluid motion from the magnetic field, thus generating very large currents in the vicinity of the x-point (near the extrema of $f(r)$). The plasma motions are heavily dumped by the restoring $\mathbf{j} \times \mathbf{B}$ force, and relax on the $\sim (\log S)^2$ time scale.

The solution of the exact dispersion relation for the $n = m = 0$ modes is compared with the asymptotic expression (24) for $10 \leq S \leq 10^{100}$, and with the decay rates obtained from the incompressible MHD simulation. For $S = 10^4$ (characteristic of laboratory plasmas) the $n = m = 0$ perturbation decay time is about 20 Alfvén times with a similar oscillation period.

For $S = 10^{10}$ (a typical value for the solar coronal plasma) the $n = m = 0$ perturbation decay time is about 120 Alfvén times and is longer than two oscillation periods. Very good agreement is seen in Fig. 4 between the nonlinear simulation with $10^2 \leq S \leq 4 \cdot 10^4$, the exact dispersion relation, and the asymptotic expression. The nonlinear terms in the MHD simulations become smaller as the perturbation decays, and the decay rates approach the linear rate (see Appendix). The asymptotic nature of Eq. (24) is evident from the figure, since agreement with the dispersion relation is improved at very large values of S.

IV. Nonlinear Simulations

A. Incompressible MHD

Now we describe results obtained by using the Alternative Direction Implicit (ADI) method to solve the incompressible MHD equations of (9) and (10) in slab geometry. The method of solution was discussed in detail in Ofman *et al.* (1991). Here we have imposed the frozen-in and ideal fluid boundary conditions in x and y-directions, respectively; namely,

$$\psi(x = \pm x_{\max}, y) = \phi(x = \pm x_{\max}, y) = \psi(x, y = \pm y_{\max}) = \phi(x, y = \pm y_{\max}) = 0 .$$

The calculations are initiated with a small perturbation ψ that is nearly azimuthally symmetric in the vicinity of the x-point in order to approximate the $m = 0$ mode. In particular we choose

$$\psi(x, y, t = 0) = b\, e^{-5(x^2+y^2)}(x_{\max}^2 - x^2)(y_{\max}^2 - y^2) , \tag{25}$$

with $b \ll 1$ and $x_{\max} = y_{\max} = 1$.

Figures 5–7 show the relaxation of an x-point with the above boundary and initial conditions. Here $S = 10^4$. In Fig. 5 plots of the energies stored in the x and y-components of the magnetic field, and the total energy are displayed as functions of time. The relaxation of the x-point proceeds at the rate predicted by the linear theory and the perturbed energies are transferred alternately between the x-component (curve A) and y-component (curve B) of

the magnetic field. The total energy (curve C) is conserved within the anticipated resistive dissipation rate. The perturbed energy stored in the magnetic field is given by

$$E_M(t) = E_{Mx} + E_{My} =$$

$$= \int_{-x\max}^{x\max} \int_{-y\max}^{y\max} \left[\left(\frac{\partial \psi}{\partial y} - y \right)^2 + \left(\frac{\partial \psi}{\partial x} + x \right)^2 - y^2 - x^2 \right] dx\, dy \ , \tag{26}$$

The perturbed kinetic energy is given by

$$E_K(t) = \int_{-y\max}^{y\max} \int_{-x\max}^{x\max} \left[\left(\frac{\partial \phi}{\partial y} \right)^2 + \left(\frac{\partial \phi}{\partial x} \right)^2 \right] dx\, dy \ , \tag{27}$$

and the total energy is given by

$$E_{\rm tot}(t) = E_M(t) + E_K(t) + E_{M0} \ , \tag{28}$$

where E_{M0},the energy stored in the initial magnetic field configuration is given by

$$E_{Mo} = \int_{-x\max}^{x\max} \int_{-y\max}^{y\max} \left[y^2 + x^2 \right] dx\, dy \ . \tag{29}$$

Because of resistive dissipation $E_{\rm tot}$ satisfies

$$\frac{dE_{\rm tot}}{dt} = -2 \int_{-y\max}^{y\max} \int_{-x\max}^{x\max} S^{-1} J^2 \, dx\, dy \ ; \tag{30}$$

we have neglected viscous dissipation since the simulation algorithm is nearly ideal [Ofman *et al.* (1991)]. The energies in Eqs. (26)-(30) are scaled by $B_0^2/8\pi$.

Figure 6 shows $\psi(0,0,t)$ (curve A), and the reconnected flux (curve B) defined by

$$\Delta\Phi(t) \equiv \int_{-x\max}^{x\max} \left| \frac{\partial}{\partial x'} \psi(x',0,t) \right| dx' + \int_{-y\max}^{y\max} \left| \frac{\partial}{\partial y'} \psi(0,y',t) \right| dy' \ . \tag{31}$$

When the initial perturbation decays, the decay rate and the oscillation frequency approach the values predicted by the linear theory. These can be determined from $\psi(0,0,t)$, or the perturbed energies. In Fig. 7 the contour lines of the total flux function $\Psi = \psi + \psi_E$ are shown at several representative times during the relaxation with $S = 10^4$. The region shown is 0.25

by 0.25 (in units of a_b) centered at the origin. Figure 7a displays Ψ at a time corresponding to a minimum of an oscillation; i.e. with negative $\psi(0,0,t)$, Fig. 7b is at a time when $\psi(0,0,t)$ is nearly zero, and in Fig. 7c $\psi(0,0,t)$ is at its maximum (see Fig. 6). The angle between the separatrices (the solid lines adjacent to the region of $\psi(0,0,t) < 0$) in Fig. 7a is larger than $\pi/2$, and in Fig. 7c is less than $\pi/2$, indicating the stressing of the magnetic configuration. In Fig. 7b the separatrices are nearly perpendicular and the magnetic configuration is close to the potential state. The oscillation is damped by the resistive relaxation, and the final state is the potential x-point configuration given by ψ_E.

B. Compressible MHD

Equations (1)–(3) and Eq. (5) were solved using the Lax-Wendroff differencing scheme, in a manner similar to that given by Richtmyer and Morton (1967), along with a smoothing term suggested by Lapidus (1967). The computation is done in polar coordinates (r,θ), in the domain $0 \leq \theta \leq \pi$, $0 \leq r \leq 1$. Equation (4) is not solved explicitly, however, the quality of the solutions can be monitored by checking that this equation is satisfied. The code was previously tested and successfully applied to other MHD problems (Steinolfson and Winglee, 1992). Here the code is used with the frozen-in boundary conditions at the outer boundary $r = 1$, $0 \leq \theta \leq \pi$, and symmetry boundary conditions at the diameter $0 \leq r \leq 1, \theta = 0,\ \pi$. The equilibrium magnetic field in cylindrical geometry is given by

$$\mathbf{B}_E = r(\sin 2\theta \mathbf{e}_r + \cos 2\theta \mathbf{e}_\theta) \ , \tag{32}$$

and the corresponding flux function is $\psi_E = -\frac{1}{2} r^2 \cos(2\theta)$. We have initiated the computations with the following perturbations: for the $m = 0$ case

$$\psi = -\frac{b}{\pi}(1 + \cos(\pi r)) \tag{33}$$

is used, while the $m > 0$ computations are initiated with

$$\psi = b r^3 (1 - r)^3 \cos(m\theta) \ , \tag{34}$$

where b is a parameter that controls the magnitude of the initial perturbation (and hence the "nonlinearity" of the initial state). The particular choices of ψ are zero at $r = 1$, and they yield a zero current at the boundary. For $m > 0$ modes ψ and j vanish also at the origin. The simulations are evolved until the magnetic field configuration reaches a steady state (i.e., relaxes to the current-free x-point).

The temporal evolution of the magnetic field at $r_i = 0.02, 0.04, 0.06, 0.08, 0.1$, and $\theta = \pi/2$ is shown in Figs. 8a–8c (curves A-E, respectively). The values shown are $\Delta B_\theta = [B_\theta(r_i, \theta, t) - B_\theta(r_i, \theta, 1)]$, where $B_\theta = -\frac{\partial \Psi}{\partial r}$, with $S = 10^4$. The fields oscillate almost in phase at r_i, and the frequency agrees well with that predicted by linear theory. The minor phase difference, and the higher harmonics are due to nonlinear effects, and can be made arbitrary small by reducing the magnitude of the initiating perturbation. In Fig. 8b the initial $m = 0$ perturbation is an order of magnitude smaller than that of Fig. 8a, and the evolution at r_i approaches that expected from linear theory. In Fig. 8c we show the temporal evolution of ΔB_θ, where the initial perturbation was $m = 2$. The frequency and the decay rate of the evolution agree with the linear theory predictions. In Fig. 9 we present the magnetic field lines of the highly nonlinear $m = 0$ perturbation. The calculation is initiated with large currents in the vicinity of the stressed x-point. After one minute the magnetic field relaxes to a nearly current-free state, with the separatrices nearly perpendicular (Fig. 9b). The rapid relaxation (compared to τ_r) to the current-free state agrees with experimental results [Bratenahl and Yeates (1970); Baum and Bratenahl (1974a,b); Baum *et al.* (1973a,b)].

V. Lyapunov Relaxation for Incompressible MHD

In this section we present a formal Lyapunov functional stability argument, which indicates that perturbations about the x-point equilibrium of (8) decay; i.e. the system relaxes back to the original equilibrium state. The arguments used are akin to those employed for the well-known Boltzmann H-theorem of kinetic theory, which demonstrates relaxation to thermal

equilibrium.

Intuition for the method can be obtained by considering a finite dimensional system of ordinary differential equations. If one can find a function, say H, defined on the state space of such a system, where contours of H are nested closed surfaces about the equilibrium point, which is a minimum, and where the time derivative $dH/dt \leq 0$ and vanishes only on the equilibrium point, then Lyapunov's theorem guarantees asymptotic stability; i.e. the trajectory of the system in proceeding to ever smaller values of H, approaches the equilibrium point as time approaches infinity.

The dynamics considered here is determined by the infinite dimensional partial differential equations of incompressible MHD, Eqs. (9) and (10), where viscous dissipation is included; i.e. $\nabla^2\omega/S_V$, where S_V is a dimensionless parameter that measures the effect of viscosity, is added to the right-hand side of (10). A general two-dimensional fixed spatial domain D is considered here (for the simulations D corresponds to the box of size $2x_{\max} \times 2y_{\max}$). Recall the ideal fluid boundary condition is:

$$\mathbf{v} \cdot \hat{n}|_{\partial D} = 0 \qquad \Rightarrow \qquad \phi|_{\partial D} = \text{constant} = 0 \ , \tag{35}$$

where ∂D denotes the boundary of the region D and $\hat{n}$ is the unit outward normal of D. When viscosity is included the appropriate additional boundary condition is

$$\mathbf{v} \cdot \hat{t}|_{\partial D} = \mathbf{e}_z \times \nabla\phi \cdot \hat{t}|_{\partial D} = \hat{n} \cdot \nabla\phi|_{\partial D} = 0 \ , \tag{36}$$

where $\hat{t}$ is the unit tangent vector to the curve defining D. For the magnetic field we made use of the frozen-in boundary condition:

$$\Psi|_{\partial D} = \psi_E \tag{37}$$

which is equivalent to

$$\psi|_{\partial D} = \text{constant} = 0 \ . \tag{38}$$

Now we will show that the following energy type functional satisfies the above requirements for Lyapunov stability:

$$H[\phi,\psi] = \frac{1}{2}\int_D \left(|\nabla\phi|^2 + |\nabla\psi|^2\right)\, d^2x\ . \tag{39}$$

The functional H is positive definite with an extremal point satisfying

$$\delta H[\phi,\psi;\delta\phi,\delta\psi] = -\int_D \left(\nabla^2\phi\,\delta\phi + \nabla^2\psi\,\delta\psi\right) d^2x + \oint_{\partial D} (\nabla\phi\delta\phi + \nabla\psi\delta\psi)\cdot\hat{n}\, ds = 0\ , \tag{40}$$

where the divergence theorem in two dimensions has been used. Note, s denotes the arc length that parametrizes the curve describing the boundary of D. Since it is assumed that ϕ and ψ are constant on ∂D, $\delta\phi$ and $\delta\psi$ vanish on the boundary and (40) implies

$$\nabla^2\phi = 0 \qquad \nabla^2\psi = 0\ . \tag{41}$$

In light of the boundary conditions, the solution of (41) is $\phi = 0$ and $\psi = 0$; i.e. the extremal point, is the unique equilibrium point $\phi = 0$ and $\Psi = \psi_E$. Evidently, the equilibrium point is a minimum, since H is positive definite. (H in fact defines a norm on the space of functions that satisfy the boundary conditions. Thus, $H > 0$ assures strong positivity, i.e. convexity.)

Now consider the time derivative of H,

$$\frac{dH}{dt} = -\int_D \left(\frac{J^2}{S} + \frac{\omega^2}{S_V}\right) d^2x + \oint_{\partial D}\left[\left(\phi\nabla\frac{\partial\phi}{\partial t} + \psi\nabla\frac{\partial\psi}{\partial t} + \phi\nabla\omega - \omega\nabla\phi\right)\cdot\hat{n} + (J\phi\nabla\psi - \omega\phi\nabla\phi)\cdot\hat{t}\right] ds\ . \tag{42}$$

Here use has been made of Eqs. (9) and (10) and again the divergence theorem in two dimensions. Because of the boundary conditions the surface terms of (42) vanish. The first term vanishes either because of the ideal conditions $\phi = 0$ or because of $\hat{n}\cdot\nabla\phi = 0$, while the second term vanishes because of the frozen condition $\psi = 0$. Similarly, the third, fifth

and sixth terms vanish because of the ideal boundary condition $\phi = 0$. However, the fourth term requires the nonideal condition $\hat{n} \cdot \nabla\phi = 0$. When these conditions are met Eq. (42) becomes

$$\frac{dH}{dt} = -\int_D \left(\frac{J^2}{S} + \frac{\omega^2}{S_V} \right) d^2x \ . \tag{43}$$

Thus we see that $dH/dt \leq 0$ and vanishes when $J = \omega = 0$, which are precisely the conditions for the equilibrium point as given by (41).

In the simulations viscosity is quite small, so small that it does not influence the dynamics during relaxation. Since the simulations were initialized with no perturbed velocity, the role of viscosity is minimal as the current decays resistively.

VI. Summary and Discussion

We have derived the linear dispersion relation for the relaxation rate of an x-type neutral point with frozen-in boundary conditions for modes with any value of m. The reconnection rate for $m = 0$ modes scales as $(\log S)^{-2}$. When the $m > 0$ modes are present large currents are generated at $r \approx r_c$, and the perturbations relax through the coupling of the fluid motions to the magnetic field via the $\mathbf{j} \times \mathbf{B}$ force. Although the $m > 0$ modes do not reconnect at $r = 0$, they can generate additional x-points away from the origin at the separatrices.

Numerical solution of the dispersion relation agrees with the asymptotic expressions for the decay rate. We have solved the nonlinear incompressible resistive 2-D MHD Equations (9) and (10) in slab geometry, using the ADI method. The computations were initiated with small nearly azimuthally symmetric perturbation of ψ, with $\phi = 0$, and large $\Delta t \sim 0.8\tau_h$, for several values of the magnetic Reynolds number in the range $10^2 \leq S \leq 4 \cdot 10^4$. We have found that the perturbations decay in agreement with the linear dispersion relation for $n = m = 0$ modes.

We have solved the compressible resistive 2-D MHD equations in the (r, θ) plane using

the Lax-Wendroff differencing scheme with $S = 10^4$, $m = 0, 1, 2$ and found that with frozen-in boundary conditions the perturbed x-point relaxes to the potential x-point in agreement with the linearly predicted rate.

By obtaining the Lyapunov functional of the current-free x-point with frozen-in boundaries we showed that this is an equilibrium configuration to which all perturbed states must relax.

The reconnection rate obtained from the linear theory and the nonlinear simulations is faster than the Sweet (1958) and Parker (1963) $\eta^{1/2}$ rate, but slower than the Petcschek (1964) Alfvénic driven reconnection rate. The $m > 0$ modes relax faster than the $m = 0$ modes for $S < 10^4$. For typical solar parameters ($S = 10^{14}$) the $m = 0$ modes reconnect and dissipate most of their energy within a hundred Alfvén times, while the $m = 1, 2$ modes have an order of magnitude longer relaxation time.

Acknowledgments

One of us (LO) would like to thank F. Porcelli for useful discussions. Another of us (PJM) would like to acknowledge a conversation with A. Hassam that instigated the calculation of Sec. V. This work was supported by the U.S. Department of Energy Contract No. DE-FG05-80ET-53088 and the National Science Foundation Contract No. ATM-90-15705.

Appendix

In this Appendix, arguments are given for why linearized compressible MHD (with $\nabla P = 0$) has the same x-point relaxation as that of the incompressible MHD.

In Eq. (11) we have assumed $\nabla P = 0$, and from linearized Eq. (5) we have to the first order

$$P \sim \rho \ , \tag{44}$$

where P and ρ are the perturbed pressure and density respectively. Hence, both P and ρ are to first order functions of time alone, which implies (with the equilibrium density $\rho_0 \equiv 1$)

$$\frac{\partial \rho(t)}{\partial t} + \nabla \cdot \mathbf{v}(x, y, z, t) = 0 \ . \tag{45}$$

Therefore $\nabla \cdot \mathbf{v}$ is to the first order a function of time alone. Since the evolution is two dimensional for both the compressible and incompressible cases ($B_z = v_z = 0$), we can separate the velocity into compressible and incompressible parts as follows:

$$\mathbf{v} = \nabla \times (\phi \mathbf{e}_z) + \mathbf{r}\, f(t) \ , \tag{46}$$

where the first term is the incompressible part, $f(t) \equiv \nabla \cdot \mathbf{v}$, and $\mathbf{r} = x\mathbf{e}_x + y\mathbf{e}_y$. Next, upon substituting $\mathbf{v}$ from Eq. (46) into Eq. (12) and taking the curl of the result yields an equation identical to the linearized form of the incompressible momentum equation (10):

$$\frac{\partial \omega}{\partial t} = -y \frac{\partial J}{\partial x} - x \frac{\partial J}{\partial y} \ . \tag{47}$$

Now, we substitute the velocity of Eq. (46) into the linearized Ampere's equation (13) and get

$$\frac{\partial \psi}{\partial t} = S^{-1} \nabla^2 \psi - \frac{\partial \phi}{\partial y} x + \frac{\partial \phi}{\partial x} y + (x^2 - y^2) f(t) \ , \tag{48}$$

where the last term on the right-hand side accounts for the departure from incompressible evolution. It is clear that this term vanishes on the separatrices of the x-point magnetic field

configuration (given by $x = \pm y$) and also at the x-point. It is also evident that as $r \rightarrow 0$ the incompressible term approaches zero at least as r^2.

Since the reconnection of the x-point in the linear stages occurs in the vicinity of $r = 0$, and as the initial perturbation decays exponentially, its relative importance becomes even more localized near the x-point, the evolution and the decay rates obtained from the linearized compressible MHD equations are expected to be in good agreement with the evolution and the decay rates obtained from the incompressible 2-D MHD equations. The agreement is found to hold numerically and is shown in Fig. 4.

References

[1]Baum, P.J., and A. Bratenahl, J. Plasma Phys. **11**, 93 (1974a).

[2]Baum, P.J., and A. Bratenahl, Phys. Fluids **17**, 1232 (1974b).

[3]Baum, P.J., and A. Bratenahl, and R.S. White, Phys. Fluids **16**, 226 (1973a)

[4]Baum, P.J., and J. Pollack, J. Appl. Phys. **44**, 163 (1973b).

[5]Bratenahl, A., and C.M Yeates, Phys. Fluids **13**, 2696 (1970).

[6]Chapman, S. and P.C. Kendall, Proc. Roy. Soc. **A 271**, 435 (1963).

[7]Craig, I.J., and A.N. McClymont, Ap. J. **371**, L41 (1991).

[8]Craig, I.J., and P.G. Watson, Ap. J. **393**, 385 (1992).

[9]Dungey, J.W. Phil. Mag. **44**, 725 (1953).

[10]Dungey, J.W. *Cosmic Electrodynamics*, pp. 98-102 (Cambridge U.P., New York, 1958).

[11]Furth, H.P., J. Killeen, and M.N. Rosenbluth, Phys. Fluids **6**, 459 (1963).

[12]Giovanelli, R.G., Mon. Not. R. Astron. Soc. **107**, 338 (1947).

[13]Hassam, A.B., Preprint UMLPR 92-046, Univ. of Maryland (1991).

[14]Lapidus, A., J. Comp. Phys. **2**, 154 (1967).

[15]Oberhettinger, F., in *Handbook of Mathematical Functions*, edited by M. Abramowitz and I.A. Stegun (Dover Publications, Inc., New York, 1972).

[16]Ofman, L., *Resistive Magnetohydrodynamic Studies of Tearing Mode Instability with Shear Flow and Magnetic Reconnection*, Univ. of Texas, Ph.D. Thesis (1992).

[17]Ofman, L., P.J. Morrison, and R.S. Steinolfson, Phys. Fluids B (1992) to appear.

[18]Parker, E.N., Ap. J. **138**, 552 (1963).

[19]Petschek, H.E., *AAS-NASA Symp. on Solar Flares*, NASA SP-50, p. 425 (1964).

[20]Priest, E.R., *Solar Flare Magnetohydrodynamics* (Gordon and Breach, New York, 1981).

[21]Richtmyer, R.D., and K.W. Morton, *Difference Methods for Initial Value Problems*, 2nd ed. (Wiley-Interscience, New York, 1967).

[22]Rutherford, P.H., Phys. Fluids **16**, 1903 (1973).

[23]Sweet, P.A., IAU Symp. **6**, 123 (1958).

[24]Steinolfson, R.S., and R.M. Winglee, J. Geophys. Res., submitted (1992).

[25]Steinolfson, R.S., L. Ofman, and P.J. Morrison, Proc. of the Chapman Conference on Micro and Meso Scale Phenomena in Space Plasmas, submitted for publication (1992).

[26]Syrovatsky, S.I., Soviet Astron. **10**, 270 (1966).

[27]Syrovatsky, Ann. Rev. Astron. Astrophys. **19**, 163 (1981).

Figure Captions

1. The initial x-point equilibrium magnetic field configuration.

2. Decay rates of the modes with $m = n = 0$, and $n = 1$, $m = 2, 4$ obtained from the solution of the linear dispersion relation.

3. The real and imaginary parts of the eigenfunctions $f(r)$ and the current $j(r)$. (a) $m = 0$, $n = 1$, $S = 10^3$, $\gamma = 0.292 + 1.248i$. (b) $m = 1$, $n = 3$, $S = 10^5$, $\gamma = 0.275 + 2.343i$.

4. Scaling of the decay rate with S for the $m = n = 0$ mode.

5. The perturbed energies of an x-point. E_{Mx} (solid line), E_{My} (long dashed line), and $E_{\rm tot}$ (short dashed line).

6. The value of $\psi(0, 0, t)$ (solid line), and the reconnected flux (dashed line).

7. Contour lines of Ψ. (a) At a time of a minimum of an oscillation ($\psi(0, 0, t) < 0$). (b) At a time of $\psi(0, 0, t) \sim 0$. (c) At a time of a maximum of an oscillation ($\psi(0, 0, t) > 0$).

8. Compressible MHD simulation results for the relaxation of the x-point with $m = 0$ initial perturbation. (a) The change of the magnetic field at r_i, $\theta = \pi/2$. (b) Same as (a) with a smaller magnitude of the $m = 0$ initial perturbation. (c) Compressible MHD simulation of the relaxation of the x-point with an $m = 2$ initial perturbation.

9. Magnetic field lines of the compressible MHD simulation. (a) The highly stressed initial stage at $t = 0.01$ min. (b) At $t = 1\,min$ the configuration is nearly current-free.

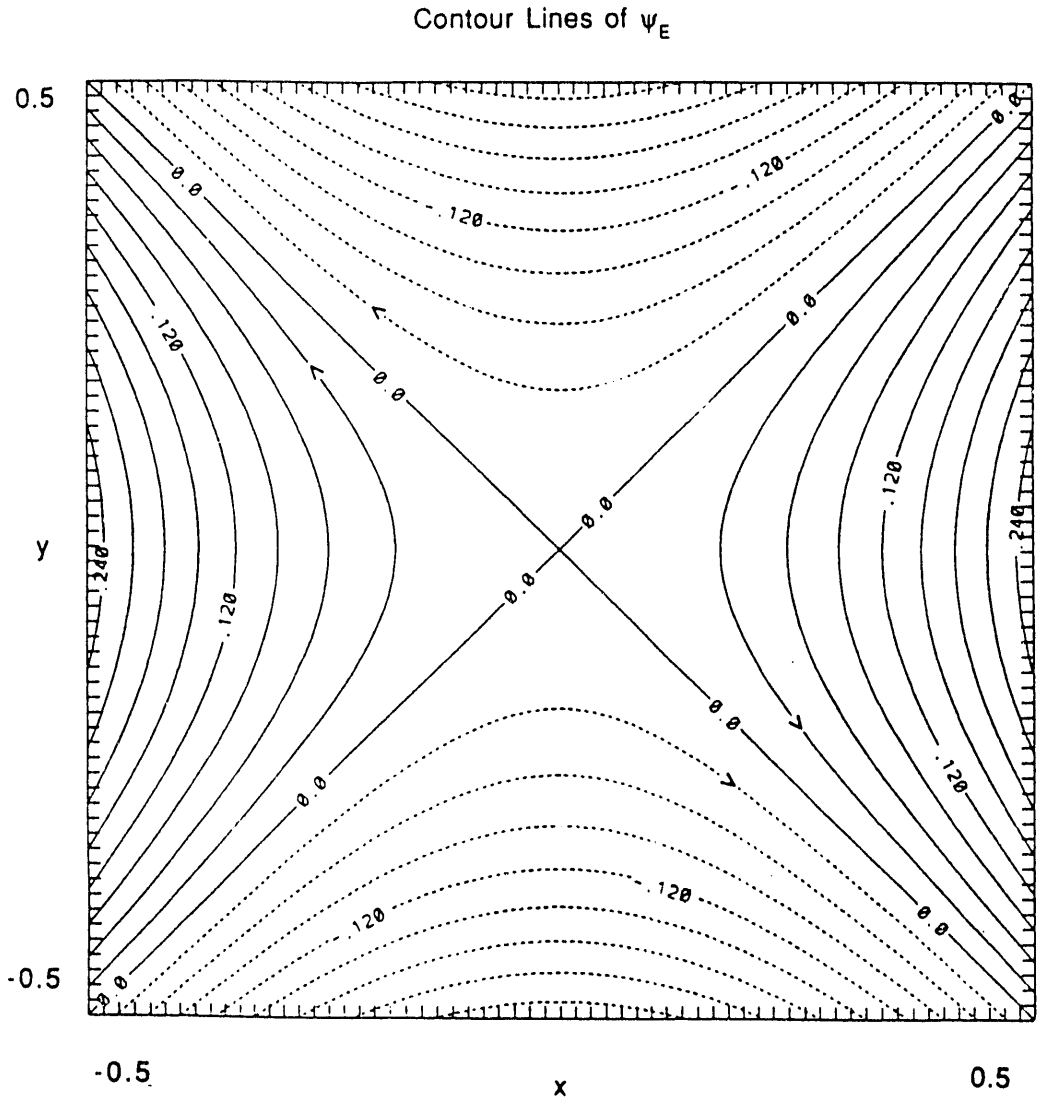

Figure 1

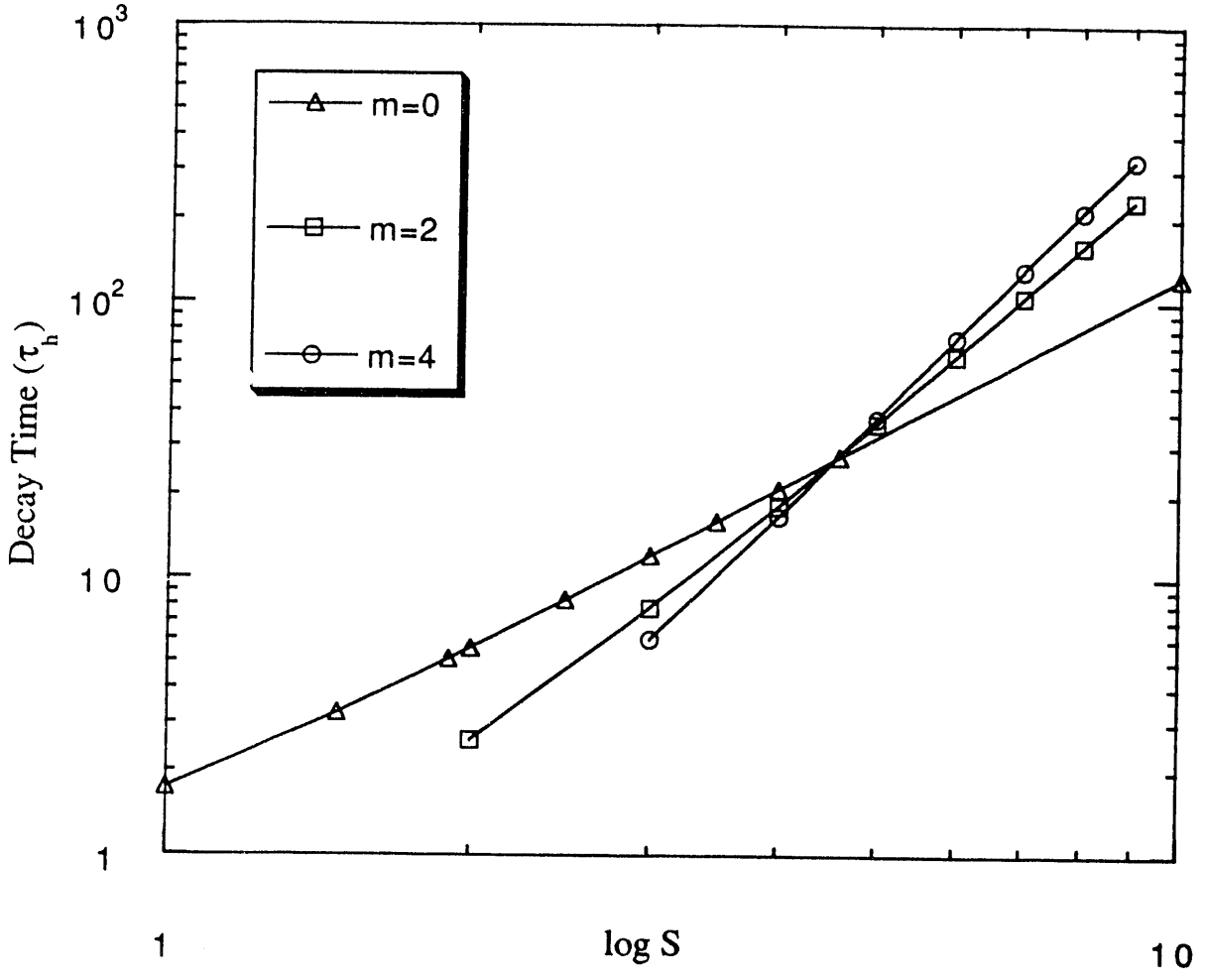

Fig. 2

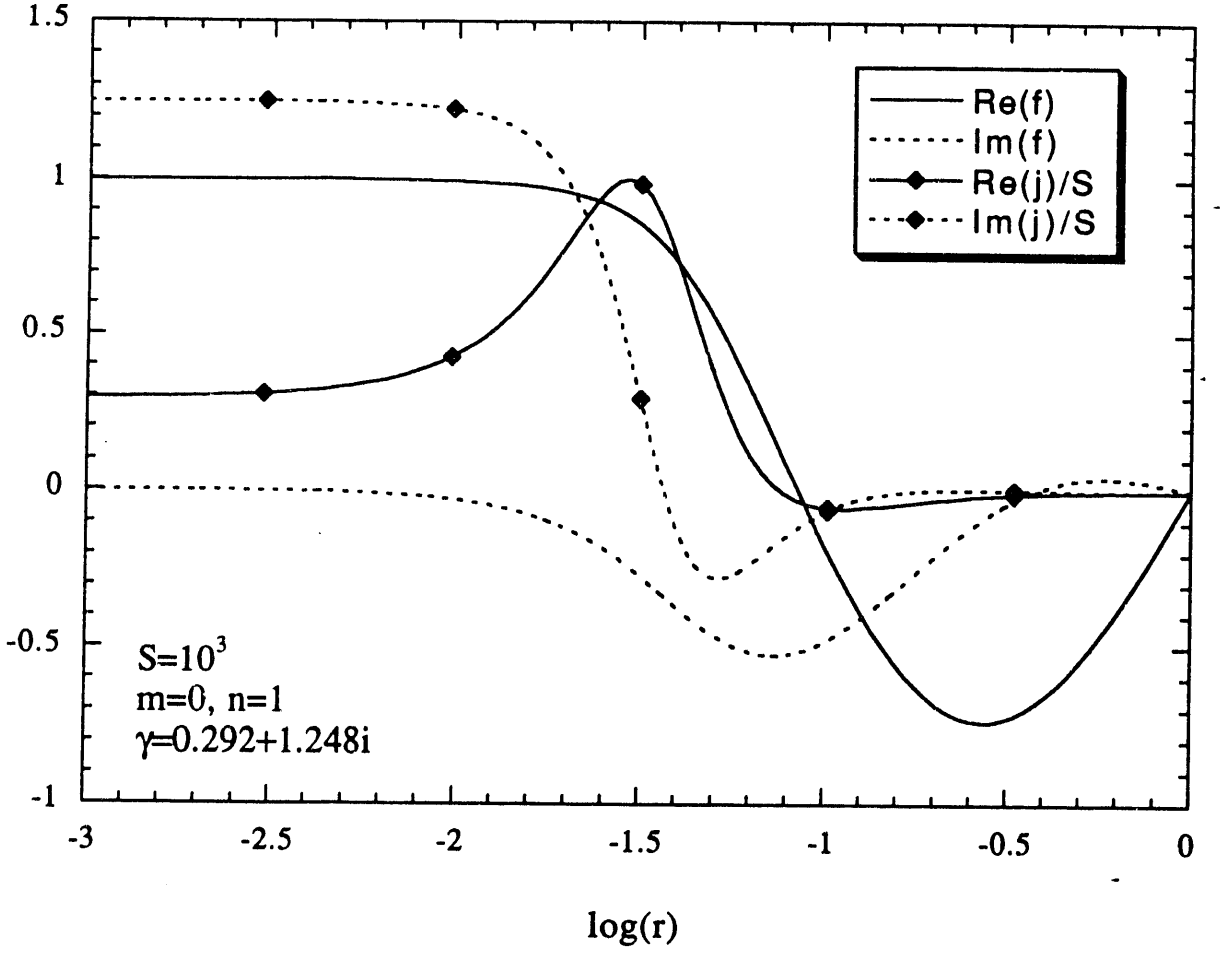
1.5
1
0.5
0
-0.5
-1
-3
-2.5
-2
-1.5
-1
-0.5
0
Re(f)
Im(f)
Re(j)/S
Im(j)/S
S=10^3
m=0, n=1
γ=0.292+1.248i
log(r)

Fig. 3a

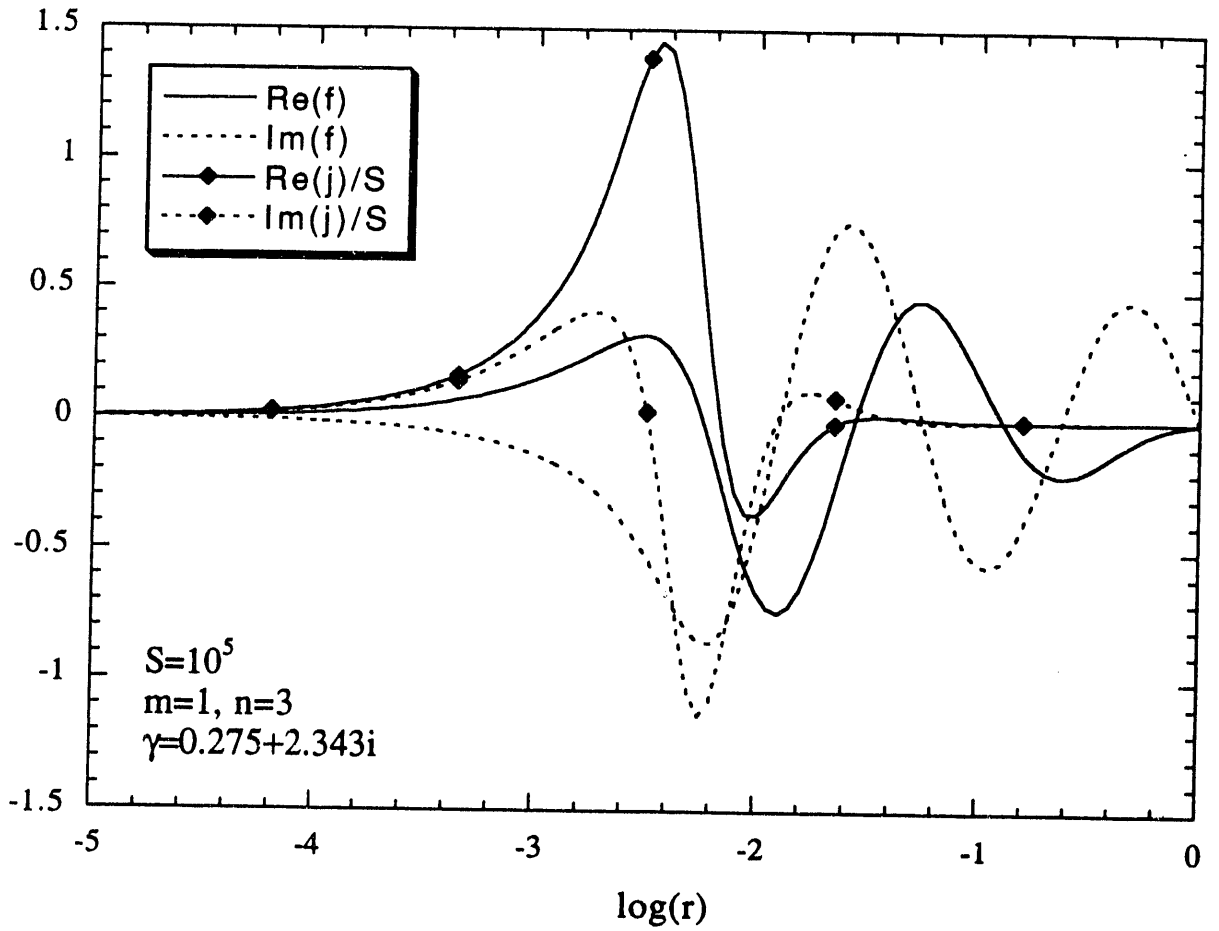
Re(f)
Im(f)
Re(j)/S
Im(j)/S
S=10^5
m=1, n=3
γ=0.275+2.343i
1.5
1
0.5
0
-0.5
-1
-1.5
-5
-4
-3
-2
-1
0
log(r)

Fig. 3b

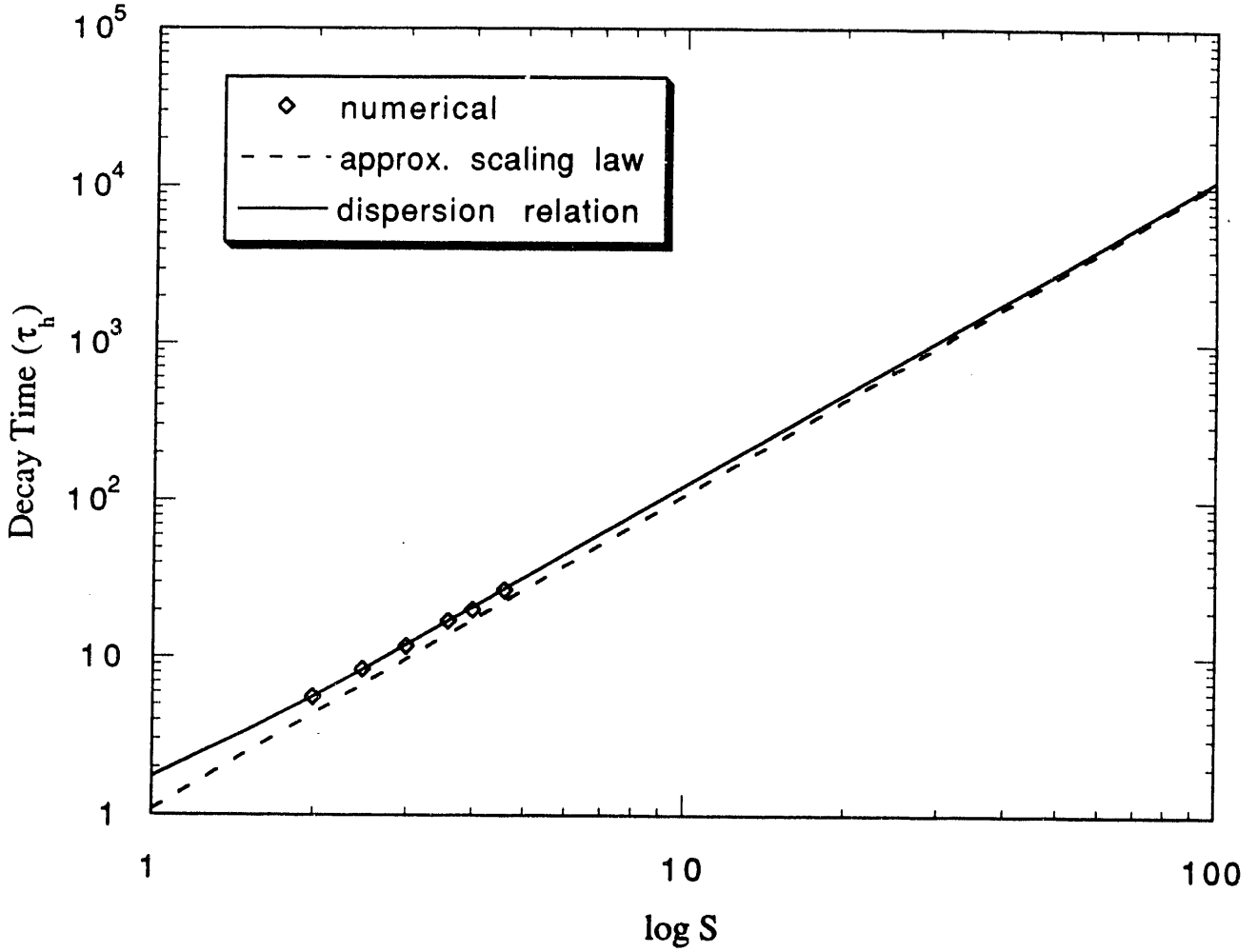
numerical
approx. scaling law
dispersion relation
Decay Time (τ_h)
10^5
10^4
10^3
10^2
10
1
1
10
100
log S

Fig. 4

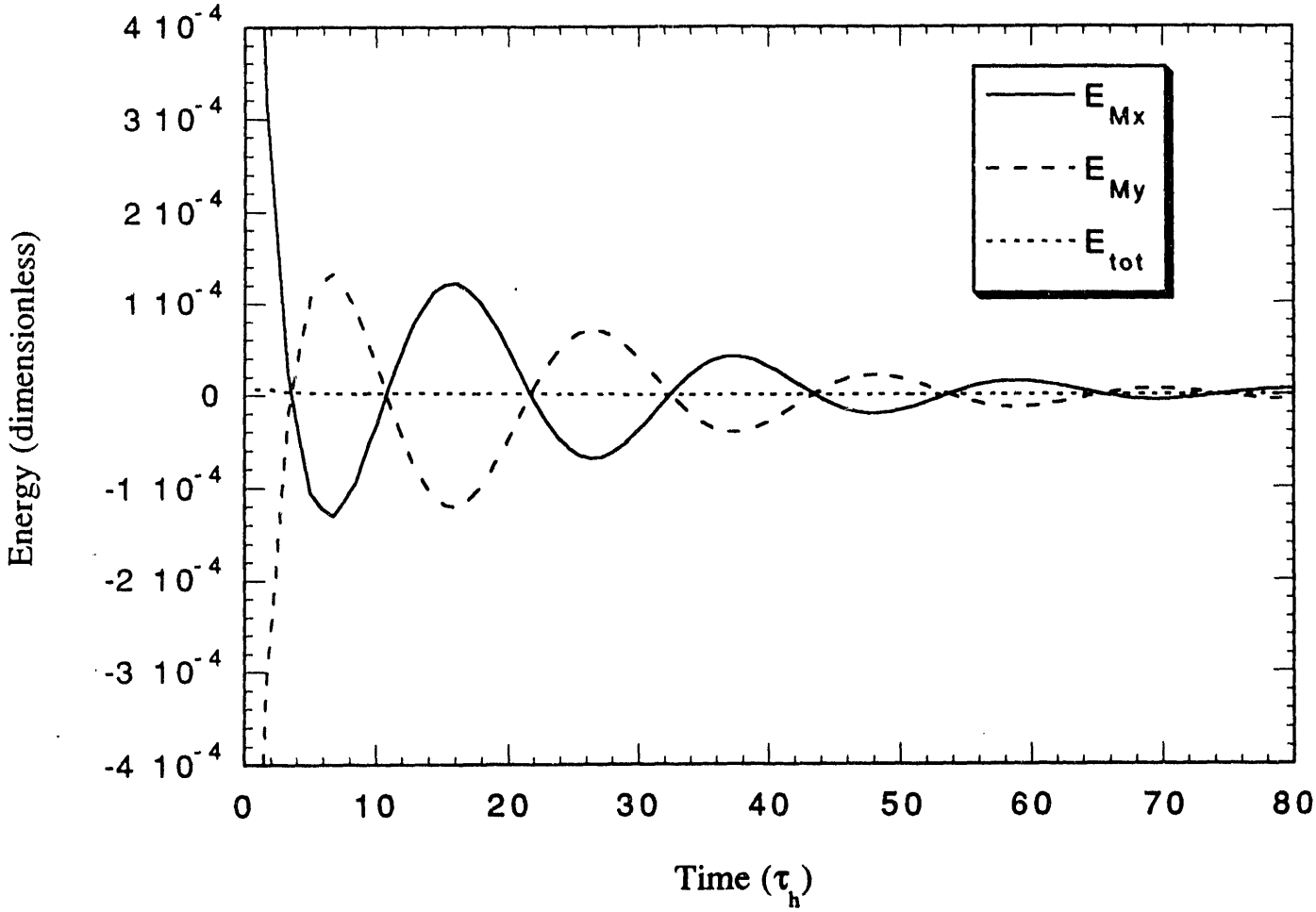
4 10-4
3 10-4
2 10-4
1 10-4
0
-1 10-4
-2 10-4
-3 10-4
-4 10-4
Energy (dimensionless)
0
10
20
30
40
50
60
70
80
Time (τh)
EMx
EMy
Etot

Fig. 5

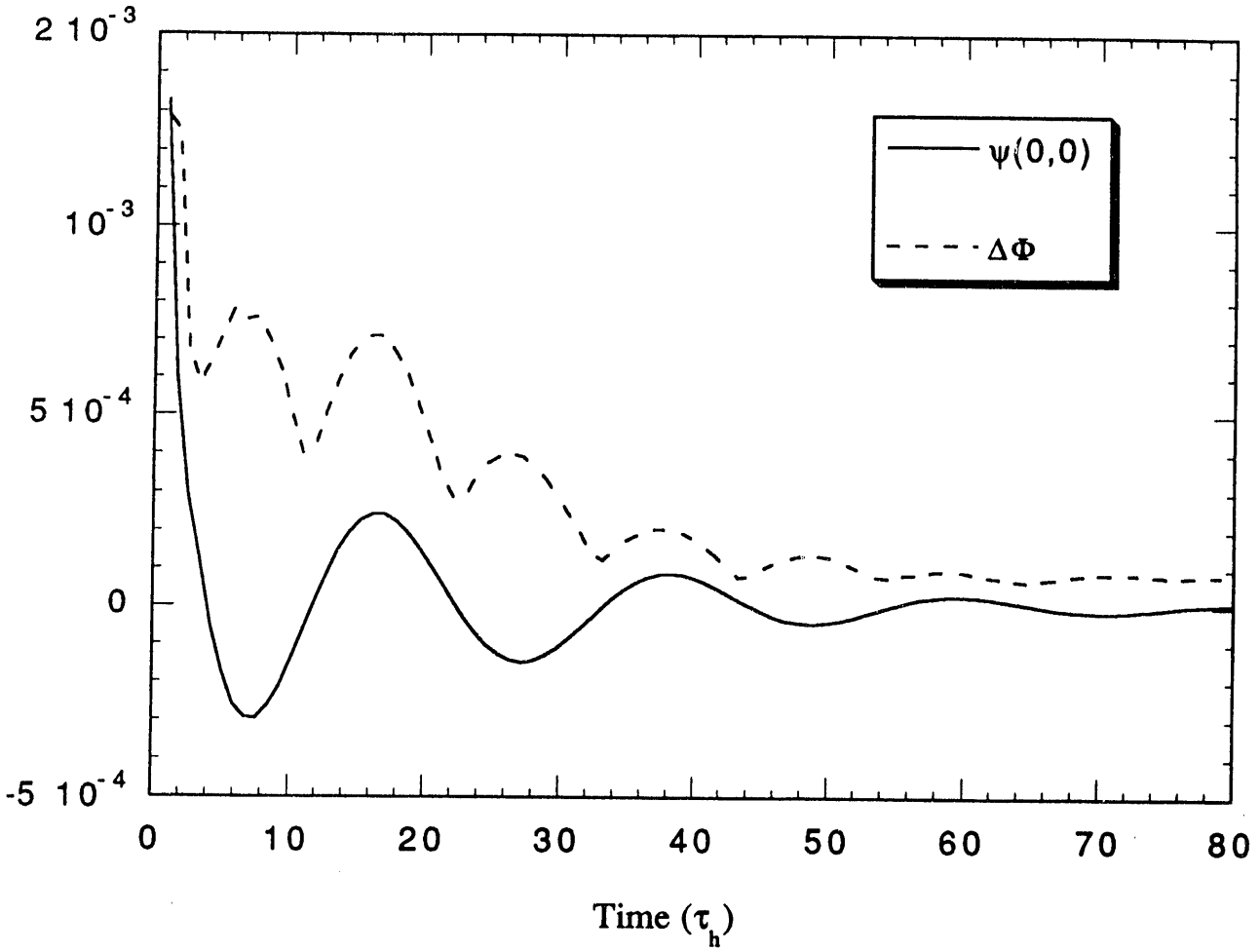

Fig. 6

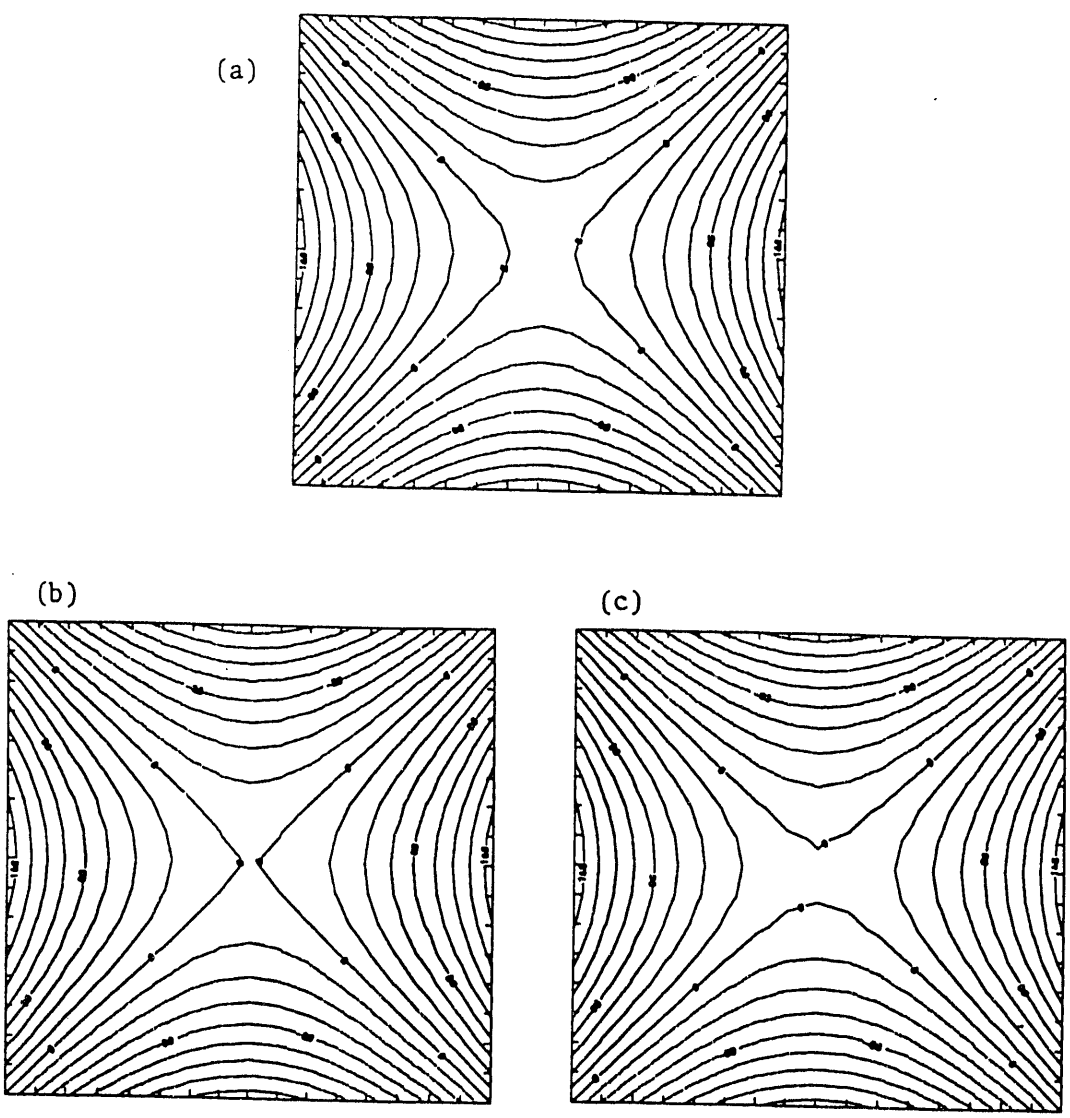

Figure 7

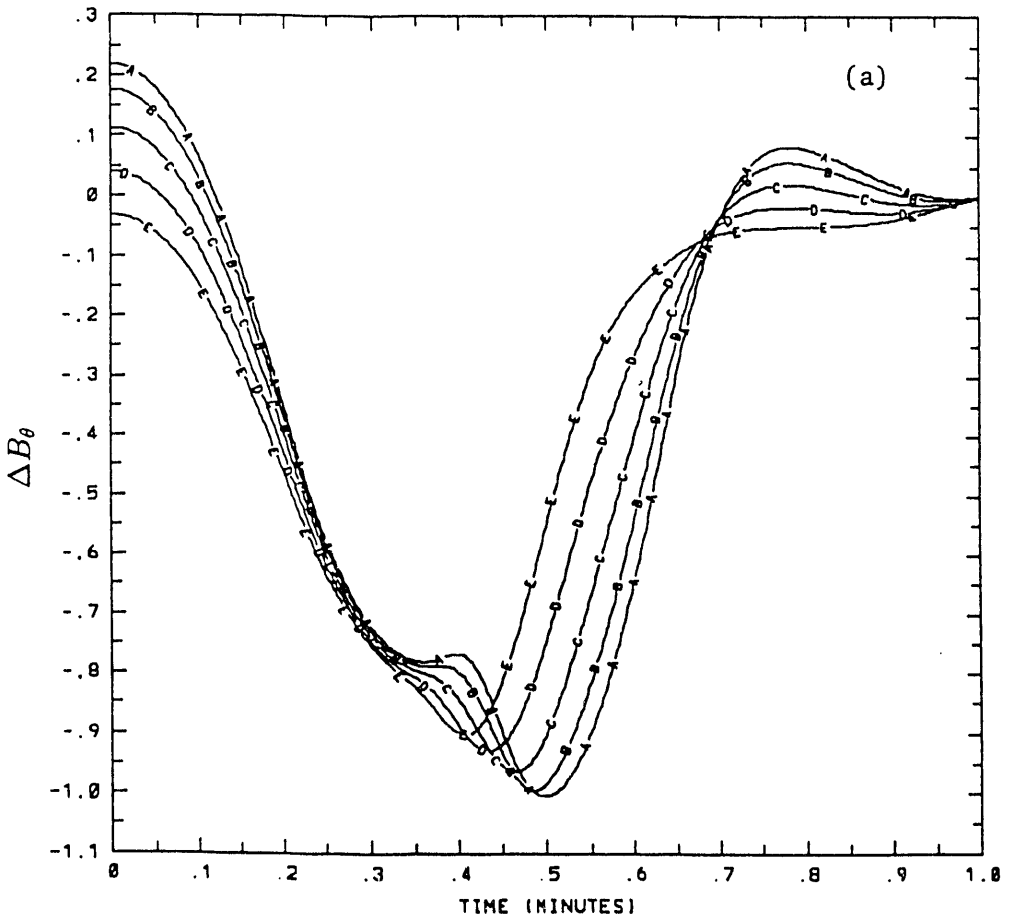
(a)
ΔB_θ
.3
.2
.1
0
-.1
-.2
-.3
-.4
-.5
-.6
-.7
-.8
-.9
-1.0
-1.1
0
.1
.2
.3
.4
.5
.6
.7
.8
.9
1.0
TIME (MINUTES)

Fig. 8a

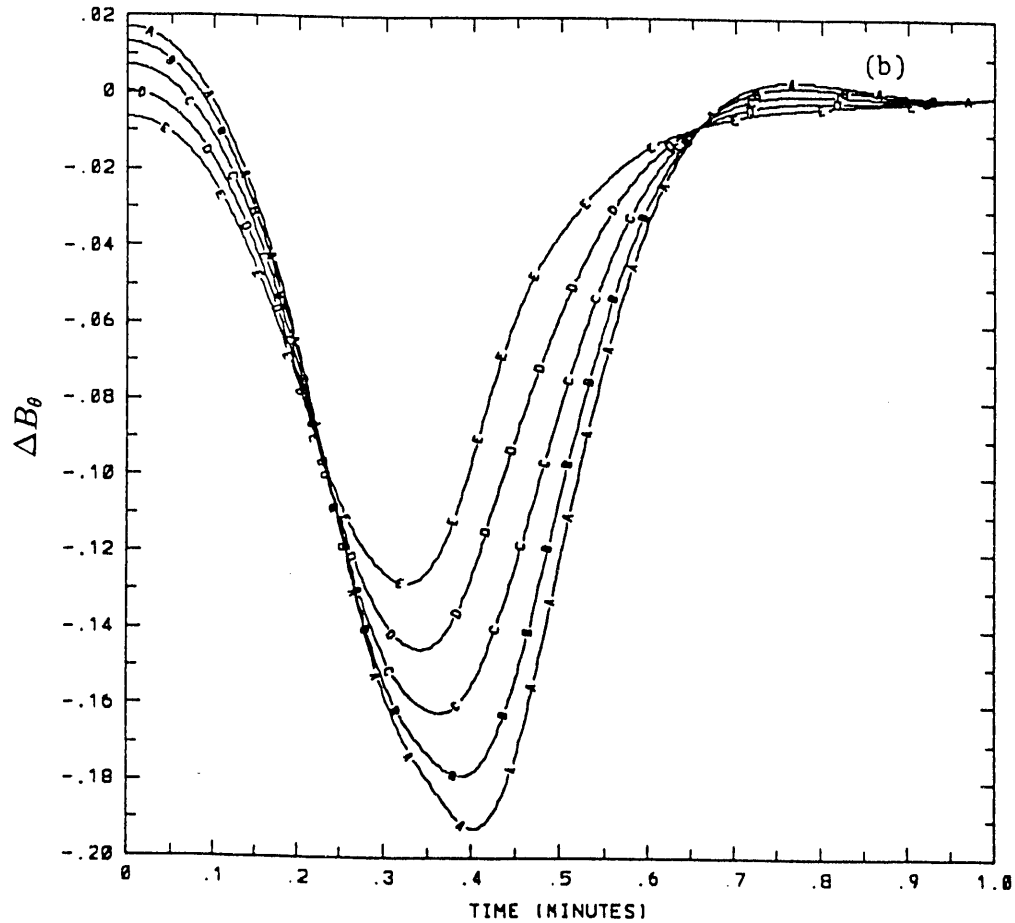
(b)
.02
0
-.02
-.04
-.06
-.08
-.10
-.12
-.14
-.16
-.18
-.20
ΔB_θ
0
.1
.2
.3
.4
.5
.6
.7
.8
.9
1.0
TIME (MINUTES)

Fig. 8b

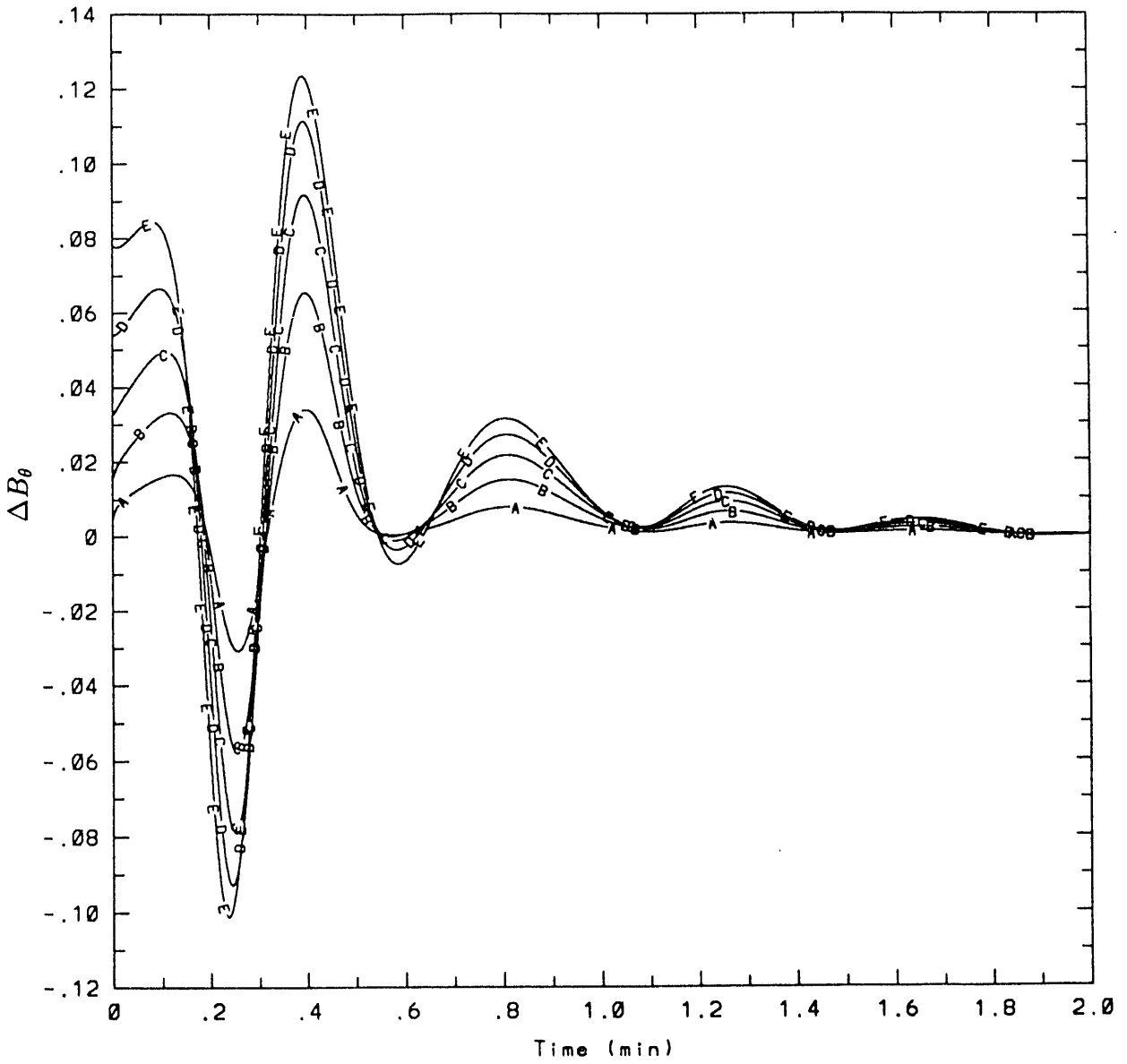
.14
.12
.10
.08
.06
.04
.02
0
-.02
-.04
-.06
-.08
-.10
-.12
ΔB_θ
0
.2
.4
.6
.8
1.0
1.2
1.4
1.6
1.8
2.0
Time (min)

Fig. 8c

time = 1.020E-02 min. magnetic field lines

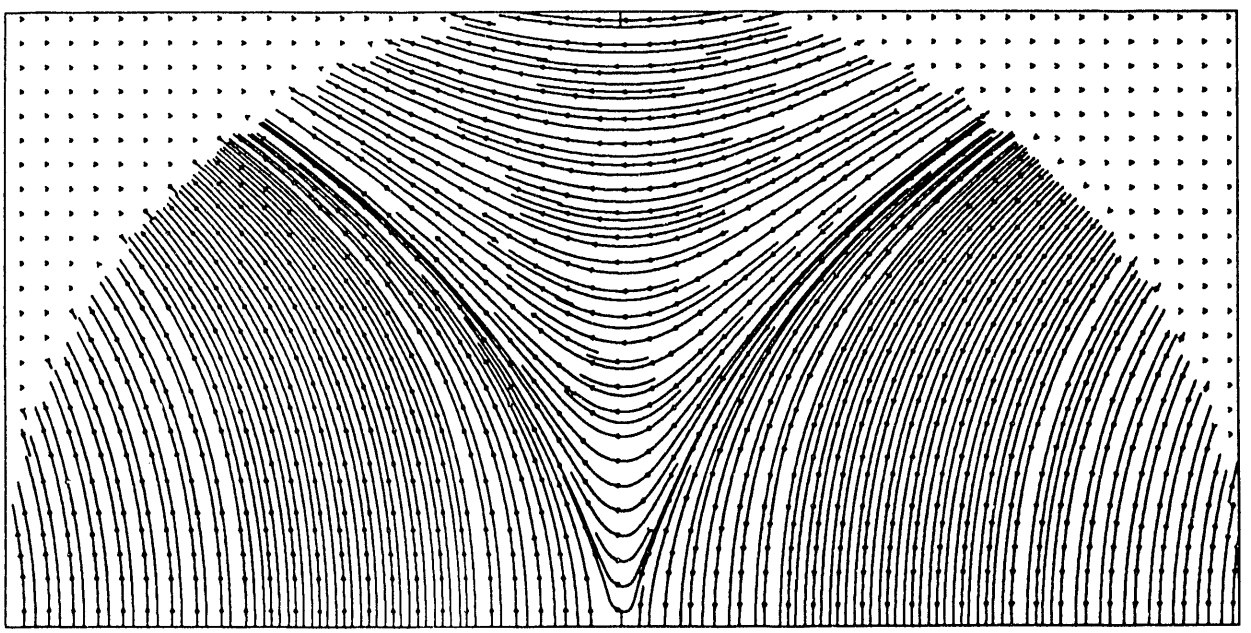

Fig. 9a

time = 1.000E+00 min. magnetic field lines

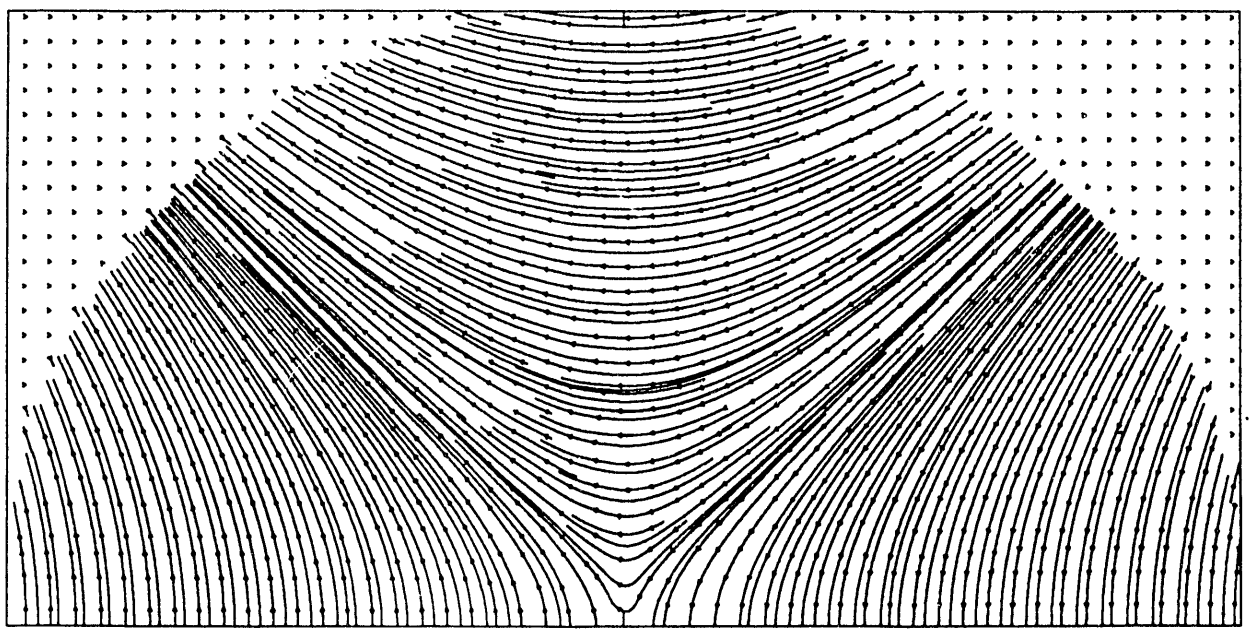

Fig. 9b

DATE
FILMED
02/02/93